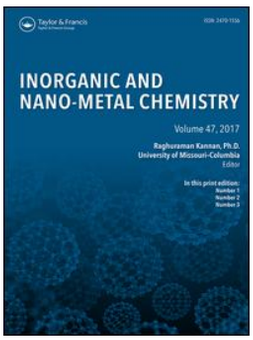

Inorganic and Nano-Metal Chemistry

ISSN: (Print) (Online) Journal homepage: https://www.tandfonline.com/loi/lsrt21

Synthesis, growth mechanism and photocatalytic properties of nickel oxide (NiO) nanoflower: a hydrothermal process

S. Virgin Jeba , S. Sebastiammal , S. Sonia & A. Lesly Fathima

To cite this article: S. Virgin Jeba , S. Sebastiammal , S. Sonia & A. Lesly Fathima (2020): Synthesis, growth mechanism and photocatalytic properties of nickel oxide (NiO) nanoflower: a hydrothermal process, Inorganic and Nano-Metal Chemistry, DOI: 10.1080/24701556.2020.1837163

To link to this article: https://doi.org/10.1080/24701556.2020.1837163

Published online: 27 Oct 2020.

INORGANIC AND NANO-METAL CHEMISTRY
https://doi.org/10.1080/24701556.2020.1837163

Synthesis, growth mechanism and photocatalytic properties of nickel oxide (NiO) nanoflower: a hydrothermal process

S. Virgin Jeba, S. Sebastiammal, S. Sonia, and A. Lesly Fathima

Research Department of Physics, Holy Cross College (Autonomous), Nagercoil, India

ABSTRACT

The present report explores the synthesis strategy of flower like Nickel Oxide (NiO) nanostructures from nanosheets as their building blocks in the presence of citric acid as surfactant. An easy and inexpensive hydrothermal technique was designed for the synthesis of NiO nanoparticles. The structural, morphological and compositional analyses were done by the techniques such as X-ray Diffraction, Field Emission Scanning Electron Microscopy and Energy Dispersive X-ray Analysis respectively and growth mechanism of the NiO nanostructure was also dealt in detail. Diffraction pattern confirms that the prepared NiO is belongs to the face cantered cubic structure. The average crystalline size was obtained by Debye Scherrer formula and the values (8 nm, 9 nm, 7 nm and 7.5 nm for NiO nanoflowers synthesized with 0.5 g, 1 g, 1.5 g and 2 g of citric acid respectively) are comparable with the size obtained by the Williamson Hall plot method. Morphological analysis confirms the formation of nanosheets constituted floral microspheres with a diameter ranging from 750 nm to 850 nm. Elemental analysis proves the presence of Ni and O and its purity. The 750 nm sized, regularly arranged NiO nanoflowers were subjected to photocatalytic degradation of Methylene Blue (MB) and Rhodamine 6G (Rh 6G) under Ultra Violet irradiation and bestow the effective degradation efficiency (76.5% and 92.6% respectively). The photodegradation mechanism was discussed based on the position of conduction and valence bands.

ARTICLE HISTORY
Received 26 May 2020
Accepted 7 September 2020

KEYWORDS
Nickel oxide; hydrothermal technique; nanoflowers; photocatalytic degradation

Introduction

Morphology controlled synthesis of nanostructured materials become an interesting research field in recent years, as they have high potential applications such as catalysts, drug delivery materials, photonic and battery materials.[1,2] Due to the exotic properties, abundance on Earth and extensive applications including sensors,[3–5] supercapacitors,[6–9] catalysts,[10,11] batteries[12,13] and electrochromics[14–16] has been reported for Nickel Oxide. Nickel Oxide (NiO) being one of the promising materials amongst the variety of transition metal oxides.[17] To enhance the device performance by exploiting the size effect, researchers developed different nano-morphologies of NiO including nanowires, nanoflowers, nanocubes, nanohexagons and nanoparticles. Among these nano-morphologies, synthesis of flower-like NiO nanostructures were reported in recent years, because of its special morphology, extremely large surface area and more number of facets which acts as active centers for electron transport. Recently, materials chemistry and device fabrication turned their focus on morphology-controlled fabrication and self-assembly of the nanoscale building blocks into complex structures.[18–25] Zhu and coworkers[26] used polyethylene glycol (PEG) as surfactant to synthesize NiO nanoflowers through microwave-assisted hydrothermal method, Wang et al, successfully synthesized the 3D rose-like NiO[27] using solvothermal reaction with sodium acetate and PEG-4000 and Justin et al[28] synthesized NiO nanoflowers by employing homogeneous precipitation method under microwave-reflux and conventional-reflux conditions using organic surfactants and urea as the hydrolysis controlling agent. These nanoflowers show multiple applications in catalysis, sensors and drug delivery as it encompass large surface area in a small structure.[29] One dimensional nanoscale materials such as nanowires and nanorods act as the building blocks for the preparation of two-dimensional or three dimensional superstructures. Whereas, the assembly of two-dimensional nanosheets act as the building blocks for the fabrication of three-dimensional structures.[30–33] The synthesis of NiO nanoflower in the reported studies were carried out for long time reaction at higher temperature and pressure or using templates or expensive chemicals as organic reagents. As the properties and applications of Nickel oxide nanostructures are highly related to their size and shape, the preparation method is an important parameter. So, a facile and effective method is desired to synthesis and investigates the properties of NiO nanoflower. Among numerous chemical methods, NiO have been prepared by a simple, low-cost and environment friendly hydrothermal technique. The synergistic effect of high temperature and pressure in hydrothermal method provides a one-step process to produce highly crystalline materials without any post

CONTACT A. Lesly Fathima leslyfathima@holycrossngl.edu.in Research Department of Physics, Holy Cross College (Autonomous), Nagercoil 629004, Tamil Nadu, India (Affiliated to Manonmaniam Sundaranar University, Abishekapatti, Tirunelveli 627012, Tamil Nadu, India).

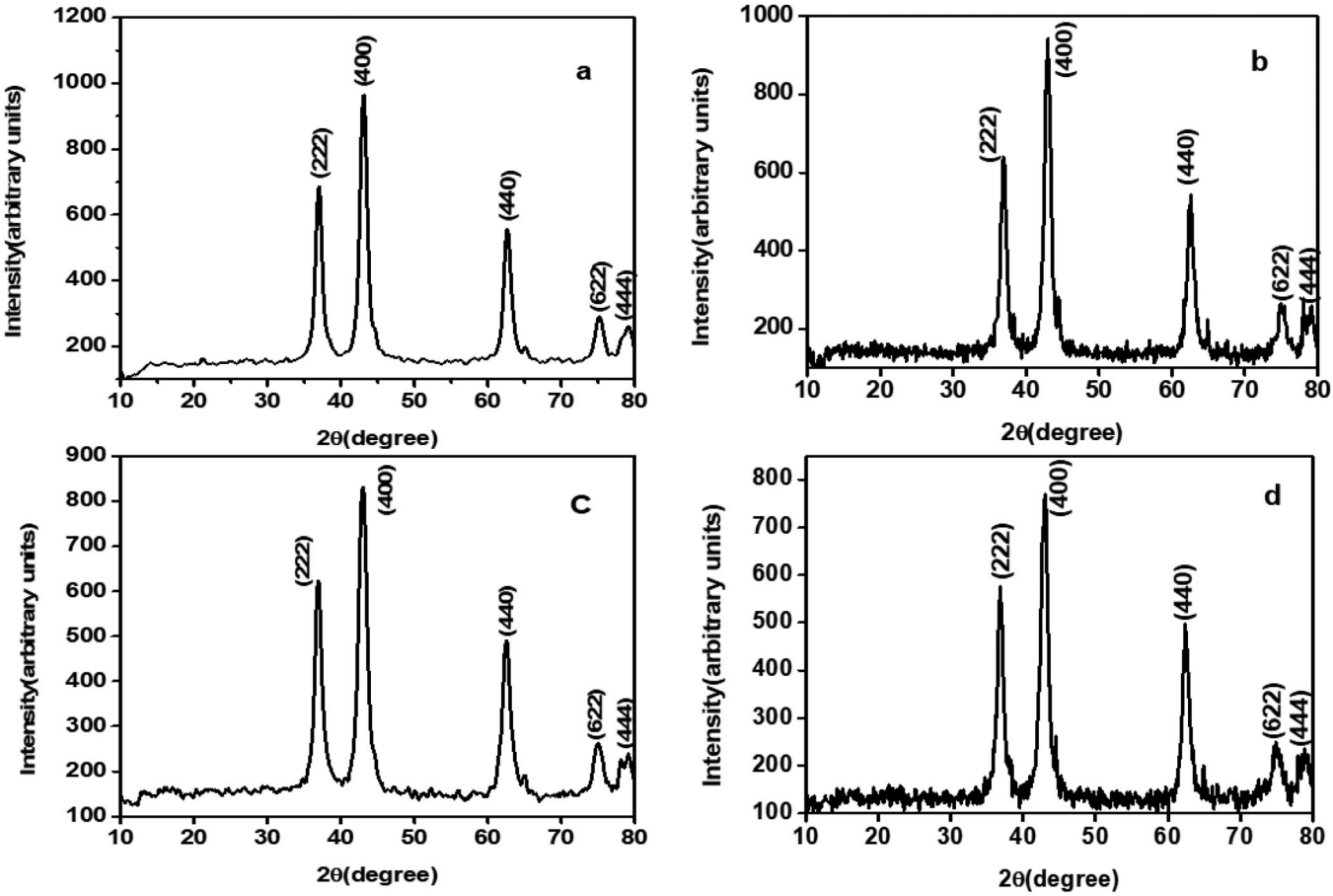

Figure 1. XRD pattern of NiO nanoflowers synthesized with (a) 0.5 g (b) 1 g (c) 1.5 g (d) 2 g of citric acid.

annealing treatments. Also, the hydrothermal treatment improves the production rate at low reaction temperature and most promising method for heterostructures synthesis.[34,35] Until now, the NiO nanoflower synthesis was carried out under high temperature and long reaction time. Thus, our work focused to synthesize the NiO nanoflowers with reduced reaction time and without templates or ligands.

In the present work, we report the synthesis strategies of flower like NiO nanostructures from nanosheets as their building blocks in the presence of citric acid as surfactant, without using hard/soft templates or other organic reagents at short reaction time. The structural analysis, morphological analysis and growth mechanism of the NiO nanostructure was also dealt in detail. The optimized NiO nanoflower was subjected to photocatalytic degradation of MB and Rh6G using the nanoflowers under UV irradiation was conducted and determined the effective degradation efficiency.

Experimental

Materials

Nickel Nitrate hexahydrate $Ni(NO_3)_2.6H_2O$, Ethylene glycol (CH_6O_2), Citric acid ($C_6H_8O_7$), ethanol (C_2H_2OH), aqueous ammonia were of analytical grade and used as received.

Synthesis of NiO nanoflowers

Nickel Oxide nanoflowers were prepared by the simple hydrothermal method. In the synthesis process of flowers, 0.3 M of $Ni(NO_3)_2$ was dissolved in DW and EG in the ratio 1:1 and aqueous ammonia was added till the pH becomes 12. Then 1 g of citric acid was added to the resultant solution and stirred for 5 hours. This homogeneous mixture was further transferred to Teflon lined stainless steel autoclave and hydrothermally treated at 180 °C for 5 hours and cooled down to room temperature naturally. The final precipitate was washed several times with distilled water and ethanol to remove the impurities and dried in hot air oven at 100 °C. Finally, the obtained powder was calcined at 400 °C for 2 hours for the transformation of $Ni(OH)_2$ to NiO.[36]

The reaction was conducted by varying the amount of citric acid used as 0.5 g, 1 g, 1.5 g and 2 g. The optimized nanostructured flowers were obtained when 1.5 g of citric acid was used. The prepared NiO nanoflower was subjected to further characterization.

Characterization of NiO nanoflowers

Structural analysis of the nanoflowers was performed by X-ray diffraction (XRD) using PANalytical XPert Pro X-ray diffractometer with monochromatic high intensity Cu-K_α radiation ($\lambda = 1.5406$ Å). The surface morphology was

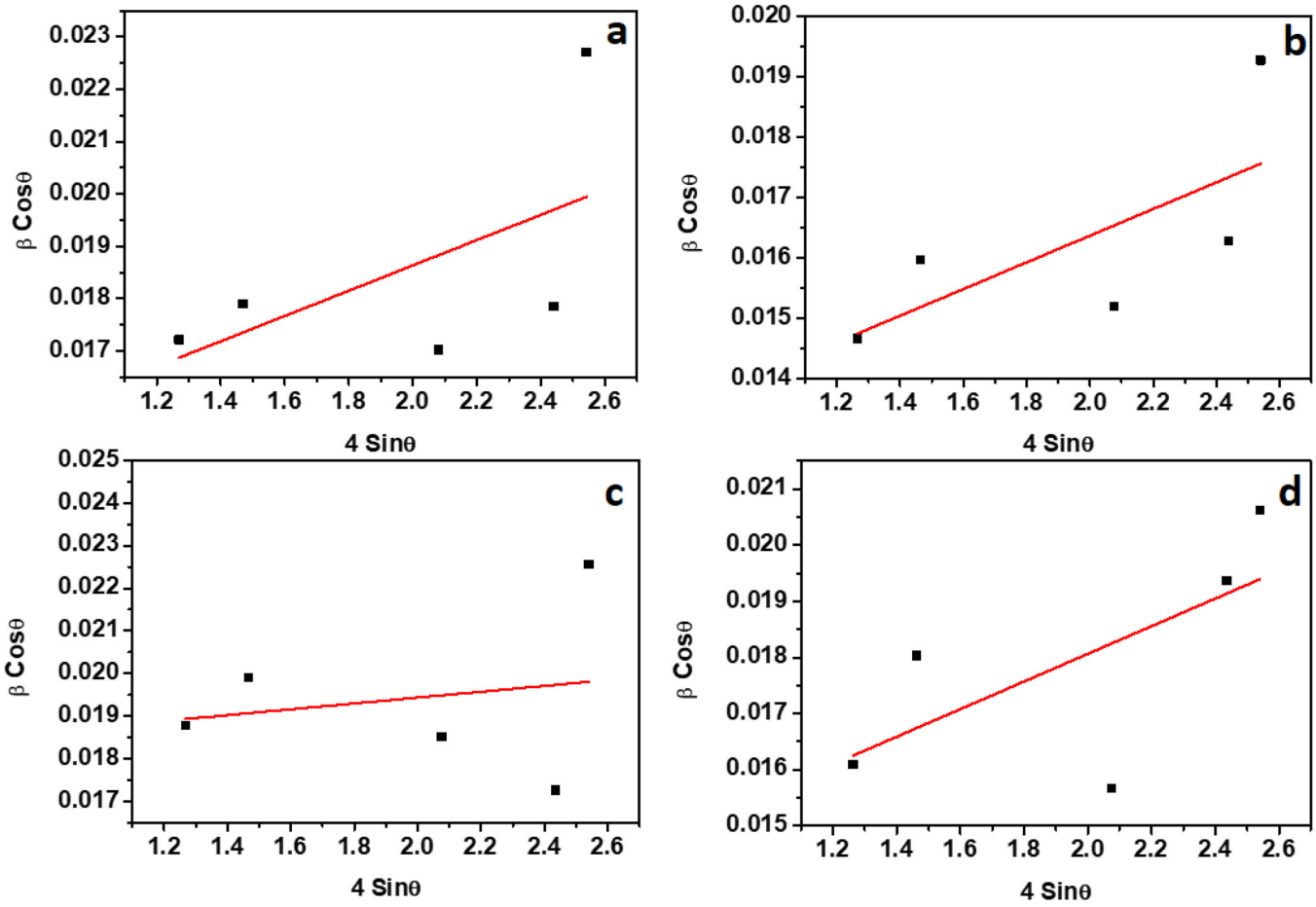

Figure 2. Williamson and Hall plot of NiO nanoflower synthesized with (a) 0.5 g (b) 1 g (c) 1.5 g (d) 2 g of citric acid.

analyzed by field emission scanning electron microscopy (FESEM) using FEI Quanta 200. Raman spectra at room temperature were obtained using LABRAM HE Evolution Micro-Raman Spectrometer. The photocatalytic degradation of the samples was examined using SYSTRONICS double beam UV-VIS spectrophotometer: 2202 in the wavelength range of 200–800 nm.

Photocatalytic activity test

The photocatalytic activities of the flowers were evaluated at room temperature using MB and Rh6G as model cationic pollutants, which are abundant in industrial effluents. In a typical procedure, 0.025 g of the photocatalyst was dispersed in 50 mL of a 2 ppm aqueous solution of MB. The solution was stirred in the dark to establish an adsorption/desorption equilibrium between the photocatalyst and the dye molecules. The solution was then illuminated by a UV source (λ_{max}=365 nm) to induce a photochemical reaction. To maintain uniform distribution, samples were collected at regular intervals and centrifuged before analysis. The same procedure was followed for aqueous Rh6G dye also. The concentration of the pollutant in the solution during the photocatalytic degradation reaction was monitored by measuring the absorbance using an UV-Vis spectrophotometer.

Results and discussion

Structural analysis of NiO nanoflowers

The typical XRD pattern of the synthesized NiO flower-like microstructure was shown in Figure 1. The formation of pure and crystalline NiO is confirmed by XRD pattern and the peaks observed were indexed with the 2θ values 39.89°, 42.94°, 62.46°, 74.92° and 78.9°corresponding to the crystallographic planes of (222), (400), (440), (622) and (444) respectively which coincides well with the standard data for NiO (JCPDS # 89-5881). All these peaks are explicitly indicates the pure FCC structure and no other peaks corresponding to secondary phase or intermediate compounds (such as $Ni(OH)_2$, Ni_2O_2, etc) was observed which demonstrate the purity of the products after calcination.

Estimation of crystallite size and lattice strain

Williamson and Hall plot is one of the most common methods to estimate crystallite size and lattice strain.[37] According to this method, the crystallite size and lattice strain can be estimated from the broadening of the X-ray diffraction peaks by considering the full width at half maximum (FWHM) of all the individual peaks. In XRD data, the broadening (β_T) of the peaks is due to the combine effect of crystallites size (β_D) and micro strain (β_e).[38]

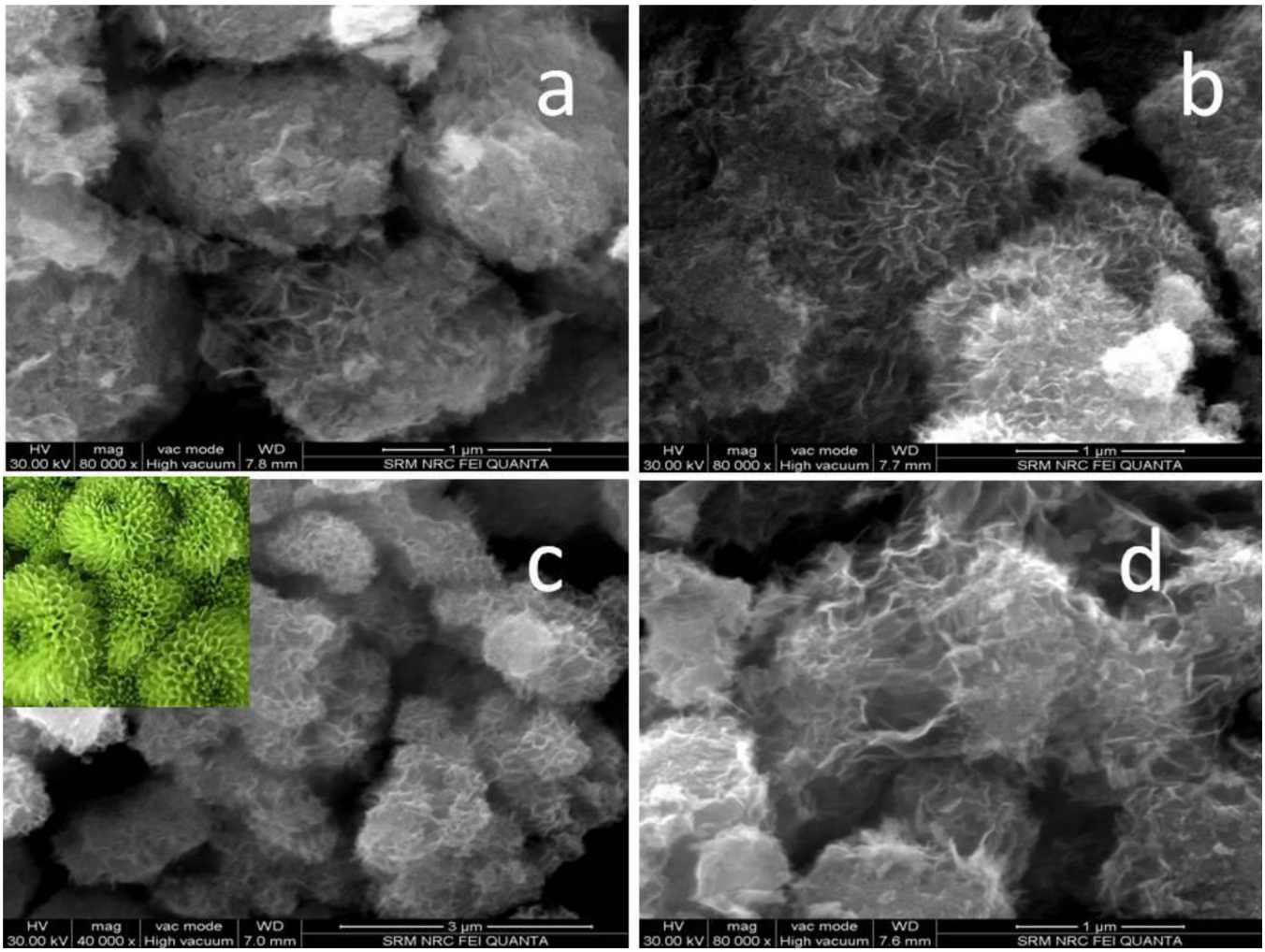

Figure 3. FESEM images of NiO nanoflowers prepared with (a) 0.5 g (b) 1 g (c)1.5g and (d) 2 g of citric acid.

$$\text{ie.})\beta_{\mathrm{T}} = \beta_{\mathrm{D}} + \beta_{\mathrm{e}} \tag{1}$$

Average crystallite size was determined from broadening of X-ray diffraction peaks by the well-known Scherrer equation is expressed as[39]

$$\beta_{\mathrm{D}} = \frac{\mathrm{k}\lambda}{\beta\ \cos\theta} \tag{2}$$

where β_D is the FWHM (i.e., broadening of the peak) in radians, k = 0.9 is the geometry factor, $\lambda = 1.5406$ Å is the wavelength of X-ray source, D is the crystallite size and θ is the peak position in radians. The average crystallite sizes of the prepared flower-like microstructures estimated by using Scherrer formula was 8 nm, 9 nm, 7 nm and 7.5 nm for 0.5 g, 1 g, 1.5 g and 2 g of citric acid in NiO nanoflower synthesis respectively. Also, the lattice parameter estimated from the XRD patterns of the samples with 0.5 g, 1 g, 1.5 g and 2 g of citric acid is 8.389 Å, 8.407 Å, 8.41 Å and 8.415 Å respectively.

Similarly, the XRD peak broadening due to microstrain is given by,

$$\beta_{\varepsilon} = 4\varepsilon\ \tan\theta \tag{3}$$

where, β_{ε} is the broadening due to strain, ε is the strain and θ is the peak position in radians. Hence we can write that,

$$\beta_T \cos\theta = \frac{k\lambda}{D} + 4\varepsilon\ \ \mathrm{Sin}\,\theta \tag{4}$$

$$\text{Or}\ \ \beta_T \cos\theta = \ \varepsilon\ (4\ \mathrm{Sin}\theta)\ + \frac{k\lambda}{D} \tag{5}$$

Equation (5) represent a straight line, in which ε is the gradient (slope) of the line and $\frac{k\lambda}{D}$ is the y-intercept. Consider the standard equation of a straight line y = mx + C and plotting (4 sinθ) on X-axis and (β_T cosθ) on Y-axis. The value of 'm' represents gradient (slope) of the line, which is the value of strain 'ε'. Williamson and Hall plots for NiO nanoflower is shown in Figure 2. A linear fit of the scattered results is taken into consideration. From this linear fit, the crystallite size was estimated from the y- intercept, and the strain, from the slope of the fit. Lattice strain is a measure of the distribution of lattice dislocations, which arises due to crystal imperfections.[40]

This W-H plotting method proved that the average crystallite size D is 10 nm, 11.6 nm, 7.6 nm and 10.5 nm for the NiO nanoflowers synthesized with 0.5 g, 1 g, 1.5 g and 2 g of citric acid respectively, which is in good agreement with the values determined by Scherer's formula. Also, the microstrain of the NiO nanoflower synthesized with 0.5 g, 1 g 1.5 g and 2 g of citric acid is about 0.00242, 0.00221, 0.000686

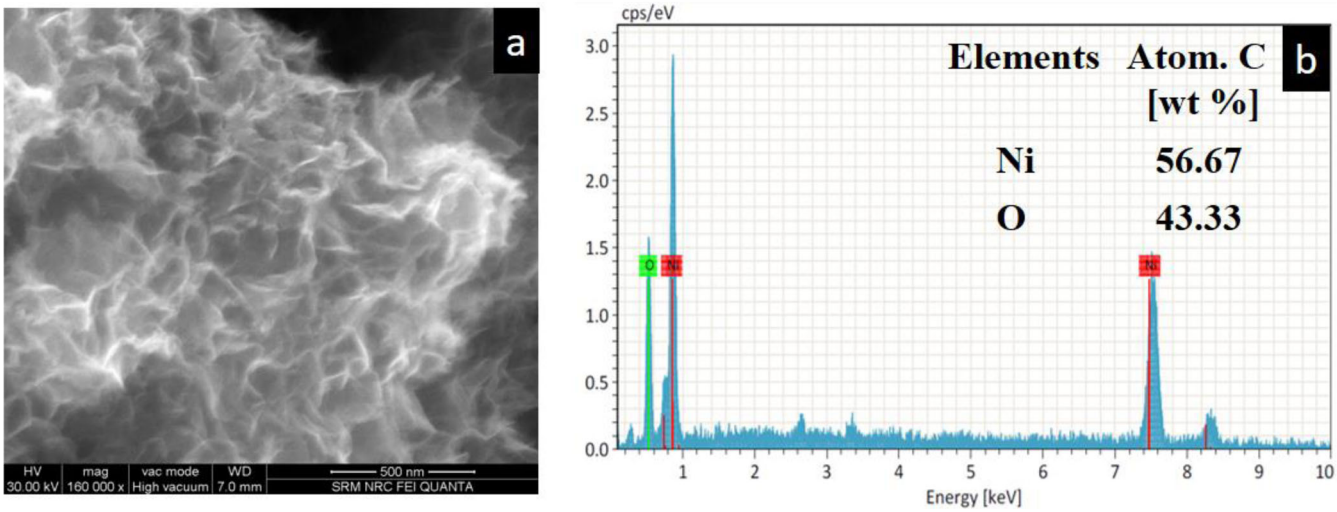

Figure 4. (a) Magnified FESEM image and (b) EDAX spectrum of the NiO nanoflower prepared at 1.5 g of citric acid.

and 0.00246 respectively, where the positive value of the lattice strain ($\varepsilon > 0$) shows that the strain in the crystal is tensile.[41]

This W-H plotting method proved that the average particle size D is 10 nm, 11.6 nm, 7.6 nm and 10.5 nm for the NiO nanoflowers synthesized with 0.5 g, 1 g, 1.5 g and 2 g of citric acid respectively, which is in good agreement with the values determined by Scherer's formula. Also, the micro-strain of the NiO nanoflower synthesized with 0.5 g, 1 g 1.5 g and 2 g of citric acid is about 0.00242, 0.00221, 0.000686 and 0.00246 respectively, where the positive value of the lattice strain ($\varepsilon > 0$) shows that the strain in the crystal is tensile.[25]

Morphological and compositional analysis of flowers

The series of FESEM images during the formation of flowers by varying the citric acid concentration in the reactions are shown in Figure 3. When 0.5 g of citric acid was introduced in the reaction system, well-defined, uniformly anchored, rough surface microspheres were formed. Also the synthesized nanopowder divulges the starting stage of the formation of flower-like microspheres as shown in Figure 3(a), whereas the addition of citric acid leads to the regular alignment of petals into flower –like morphology as shown in Figure 3(b). Figure 3(c) displays the panaromic image, from which it is seen that the typical NiO is composed with numerous flower like micro-spheres also an increase in the number of flower-like microspheres with a diameter ranging from 750 nm to 850 nm, when 1.5 g of citric acid is added. The magnified image (Figure 4) of flower like microspheres evidently explain that these spheres are composed of densely packed irregular sheets, which form a multilayered structure. The flowers deformed slightly during the addition of 2 g of citric acid.

The EDAX results of the chemically derived NiO nanoflower showed the presence of Ni and O elements as shown in Figure 4. The chemical compositions (Ni-56.67% & O-43.33) have been listed in the table (inset). In addition, there was no evidence of impurities or residues observed in the EDAX results, which also confirmed the complete formation of NiO nanostructures.

Raman analysis of NiO nanoflowers

Raman spectroscopy (Raman analysis) is an optical spectrometry highlighting the molecular vibrations, used to determine the chemical structure of a sample and allow us to identify organic molecules, polymers, biomolecules and inorganic compounds also. Figure 5 represents the Raman spectrum of the NiO nanoflowers where the band positions are expressed in (cm^{-1}) which correspond to the characteristic vibration frequencies of the molecular bands, as a function of the intensity of these bands is expressed in arbitrary units (a.u)

The Raman scattering spectra of NiO nanoflowers are shown in Figure 5. Since the first-order Raman scattering is forbidden in face-centered cubic (FCC) structure, the intensity of one-phonon scattering is expected to increase significantly in defect-rich NiO (the band at $\sim 500\,cm^{-1}$). The vibrational peak at $\sim 500\,cm^{-1}$ is assigned to the Ni–O stretching mode, which involves Ni^{2+} and O^{2-} species.[42] The increase in intensity of the one-phonon mode Raman scattering peak indicates the structural imperfection of NiO, which is due to the structural disorder by nickel interstitial, surface effects and oxygen vacancies.[43–45] In the present study, there appears smaller intensity of the one-phonon band for the nanocrystalline NiO. However, a significant gain of the one-phonon band intensity was observed by us for smaller NiO nanoparticles. Thus, an increase of surface/bulk ratio and of defect concentration is responsible for the large intensity of the one-phonon band at $\sim 500\,cm^{-1}$.[46]

There appears a strong 2LO phonon mode at $\sim 1100 cm^{-1}$ attribute to the vibration of Ni–O band. In the given Raman spectra, two magnons (2 M) excitation peak was not observed, which normally located at $1550\,cm^{-1}$ to indicate that the synthesized NiO nanoflowers does not have antiferromagnetic properties at room temperature (RT).[47,48] This drastic decrease in intensity of the two magnon band in the NiO nanoflowers with crystallite size less

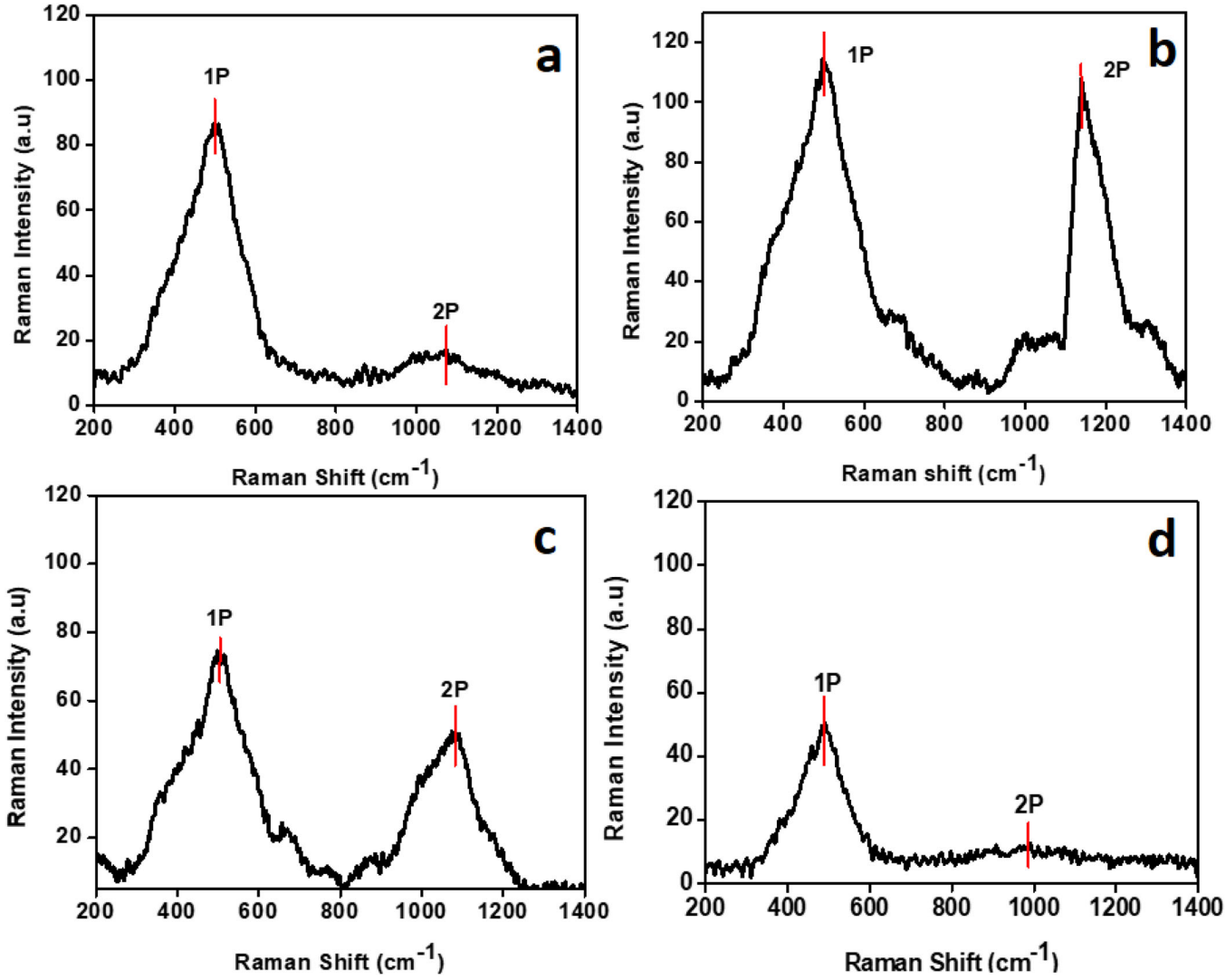

Figure 5. Raman spectra of NiO nanoflowers synthesized with (a) 0.5 g (b) 1 g (c) 1.5 g and (d) 2 g of citric acid.

than 100 nm is attributed to a decrease of antiferromagnetic spin correlations between individual Ni^{2+} ions. Also, this result indicates that due to the small crystallite size and high density of structural disorder, the NiO nanoflower exhibits super-paramagnetic properties.[46] These results indicate the crystal quality and they are in agreement with the XRD results obtained.

Optical properties of NiO nanoflowers

UV-Vis absorption spectrum is used to study the electronic structure of optical band gap of material. Figure 6 shows the optical absorption spectra of the optimized NiO nanoflower synthesized with 1.5 g of citric acid as surfactant and inset shows the corresponding Tauc's plot. A strong absorption peak is obtained in the UV region at 248.5 nm wavelength, which may be associated to the absorption band of NiO. The optical bandgap energy (E_g) can be calculated on the basis of the optical absorption spectra by the following equation:

$$\alpha h\nu = A\ [h\nu - E_g]^n \quad (6)$$

where α is the absorbance coefficient, E_g is the optical band gap energy of the material, $h\nu$ is the photon energy and n depends on the type of transition; n is either 2 for direct band gap or ½ for indirect band gap. The graph of $[\alpha h\nu]^2$ as a function of $h\nu$ is plotted for direct allowed transition. The optical bandgap of optimized NiO nanoflowers would be obtained by extrapolating the linear portions of the $(\alpha h\nu)^n$ vs $h\nu$ curve to zero[49] as shown in Figure 6. The bandgap value is found to be 3.9 eV for the optimized NiO nanoflower.

Growth mechanism of NiO nanoflowers

The mechanism involved in the synthesis of flower-like microspheres was proposed as follows: An aqueous NH_3 is added into $Ni(NO_3)_2.6H_2O$, transparent green color solution is formed due to the formation of $[Ni(NH_3)_4]^{2+}$ complex. By the further addition of citric acid, transparent green color solution turned into green color precipitate. In the presence of aqueous NH_3 the carboxylic group of citric acid oxidized into carboxylate ion and being a reducing agent, the

complex ion $[Ni(NH_3)_4]^{2+}$ reduces into Ni atom.[50] Finally the product generated is $Ni(OH)_2$, that might be due to the presence of H_2O. Then $Ni(OH)_2$ is converted into NiO at 400 °C (calcination temperature). The equations are given below

$$Ni(NO_3)_2 + CH_8O_7.H_2O + NH_3 \rightarrow 2Ni(OH)_2 + 2N_2 \uparrow + 6CO_2 \uparrow + H_2 \uparrow + H_2O \quad (7)$$

$$Ni^{2+} + 6NH_3 \rightarrow [Ni(NH_3)_6]^{2+} \quad (8)$$

$$NH_3 + 2OH \rightarrow NH^{4+} + OH^- \quad (9)$$

$$Ni^{2+} + 2OH^- \rightarrow Ni(OH)_2 \uparrow \quad (10)$$

$$Ni(OH)_2 \xrightarrow{400^\circ C} NiO \quad (11)$$

After reaction for 0.5 g of citric acid, the product was morphogenetic microspheres with coarse surfaces. The particles of the microspheres aggregate and grow into inhomogeneous nanosheets, when the amount of citric acid increased to 1 g. Also it was observed intuitively that small nanosheets began to appear on the surface of the microspheres. When the treatment was further increased to 1.5 g these superficial nanosheets, with the attachment of small particles, grew and overlapped each other to form interconnected porous flower like microspheres by electrostatic, vanderwaals forces, hydrogen bonds etc.[51] Finally, the NiO flower-like microspheres with abundant nanoparticles adhering to the petals are obtained.

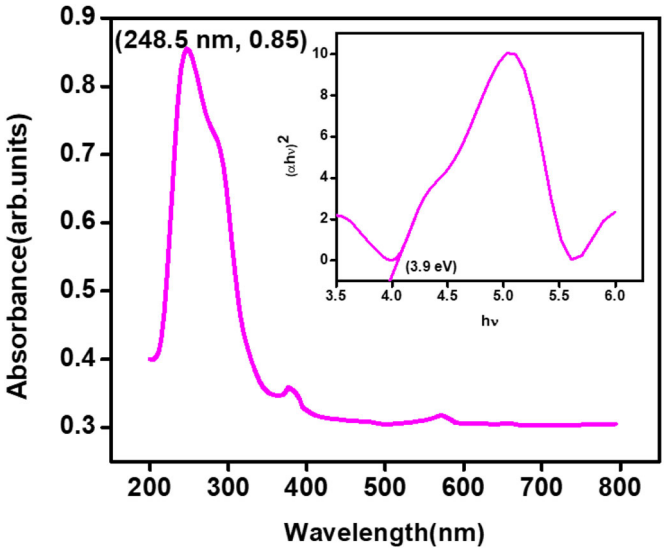

Figure 6. Optical absorbance spectra of the NiO nanoflower prepared with 1.5 g citric acid and inset shows the corresponding Tauc's plot.

Photocatalytic activity of NiO nanoflowers

Photocatalytic degradation mechanism

The most probable mechanism for the photocatalytic degradation of MB and Rh6G organic dyes is proposed as follows: The photocatalytic activity of the wide band gap NiO nanoflower photocatalyst under UV irradiation occurs when UV light with energy higher than its band gap creates electron-hole pairs (excitons).[52–54] The generated electron moves up to the conduction whereas the hole drifts in the valence band. When the photogenerated charge carriers absorbed on the surface of the photocatalyst they initiate redox reactions in toxic complex dye molecules to degrade them. The positive-hole and negative-electron of the photocatalyst react with the water molecule to form hydroxyl radicals (OH), superoxide anions (O_2^-), hydrogen peroxide molecules (H_2O_2), the hydrogen dioxide anion (HO_2^-), and hydroperoxy radicals (HO_2).[55,56] The target pollutants were degraded by these superoxide radicals and hydroxyl radicals. The formation of these superoxide anions and hydroxyl radicals – both responsible for the degradation of the organic compound, at the NiO nanoflowers-dye solution interface after the production of electron-hole pairs by UV irradiation can be summarized as follows in Figure 7.

The band gap position (CB and VB) for NiO was calculated by applying the following equations,

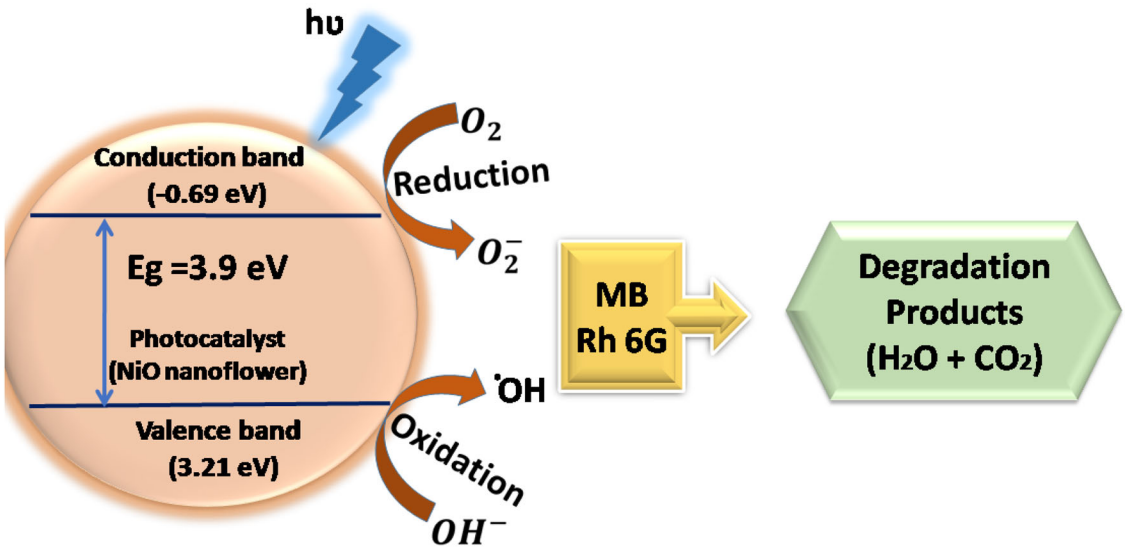

Figure 7. Schematic illustration of photocatalytic degradation of MB and Rh6G using NiO nanoflowers.

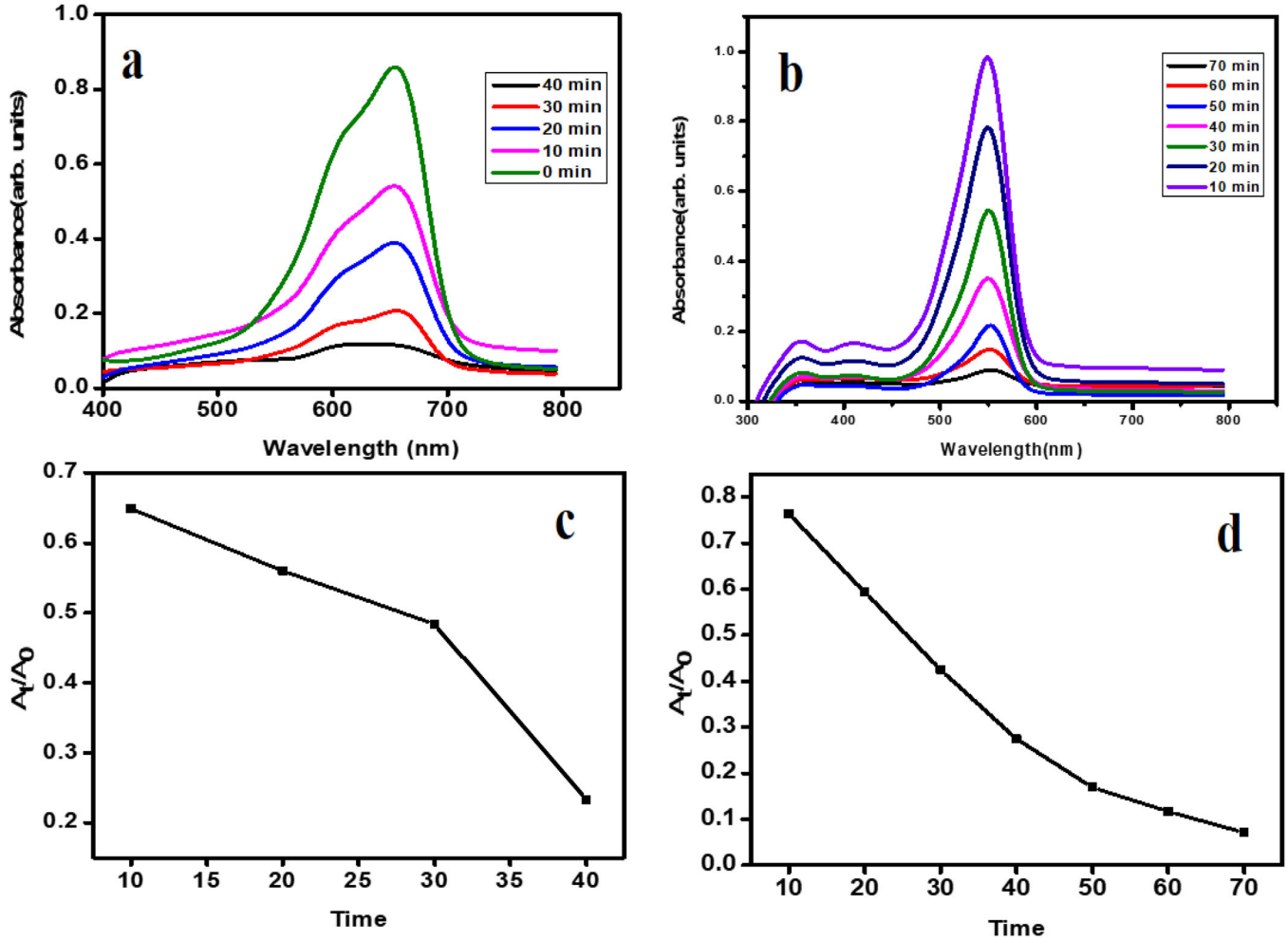

Figure 8. Photodegradation absorption spectra of NiO nanoflowers for a) MB, b) Rh6G and Photodegradation efficiency of NiO nanoflowers for c) MB, (d) Rh6G.

$$E_{CB} = X - E^e - 0.5\ E_g \quad (12)$$

$$E_{VB} = X - E^e + 0.5\ E_g \quad (13)$$

where E_{CB} and E_{VB} are the conduction band and valence band edge potentials, X is the electronegativity of the semiconductor (NiO is 5.76 eV),[57–64] E^e is the energy of free electrons on the hydrogen scale (4.5 eV) and E_g is the bandgap of NiO (3.9 eV) calculated from Tauc plot. The calculated conduction and valence band position of NiO are −0.69 eV and 3.21 eV respectively. The electrons transferred from CB of NiO can able to generate O_2^- by photo-reduction of dissolved O_2 due to its less positive CB edge potential (−0.69 eV) compared to O_2 reduction potential (−0.33 eV). Also, the reduction potential of O_2 is 0.695 eV, the electrons can react with O_2 and H^+ to generate highly reactive *OH. The VB holes in NiO can generate *OH by reacting with H_2O and –OH due to its favorable VB potentials. Since the prepared NiO nanoflower catalyst having the ability to generate all of these active species (*OH and h^+) and which are highly oxidizing in nature and leads the degradation of pollutants into CO_2 and H_2O. Due to the high work function of NiO (5.2 eV),[65] electrons excited to the conduction band are easily transferred to the chosen dye and produce H_2O_2 which will decompose the dye under UV light illumination.

The high surface area of NiO nanoflowers can provide more active absorption capacity. Ni ions produce hydroxyl groups by absorbing water in the air. When light falls on the sample, the electrons gets shifted from valence band to conduction band and thus creates electron-hole pair.[66] This results an increase in the photocatalytic activity as shown in Figure 8.

Photocatalytic studies

Photodegradation experiments were conducted using cationic dye solutions of MB and Rh6G with and without NiO nanoflowers (photocatalyst) under an UV irradiation source at room temperature.

The degradation efficiency of the NiO nanoflowers was calculated using the formula:

$$\text{Degradation efficiency, } \eta\ (\%) = (A_o - A/A_o)\ \text{x}\ 100 \quad (14)$$

where A_o is the absorption maximum at t = 0 and A is the absorption maximum at time $t - t_{min}$.[67]

The absorption spectra obtained for MB and Rh6G as well as their concentrations in solution when sampled at regular intervals of 10 min are presented in Figure 8(a, b). From Figure 8(a, b) it is evident that the absorption peaks

of both the dyes decreased gradually as the exposure time increased from 0 to 40 min and 0 to 70 min for MB and Rh6G respectively. With the increase of irradiation time, the intensity of the maximum adsorption peak located near 664 nm and 550 nm for aqueous MB and Rh6G dyes respectively gradually decreased, indicating the degradation of the dye solutions. Thereby it demonstrates the ability of the NiO nanoflowers to effectively degrade various cationic dyes.

The degradation efficiency of the NiO nanoflowers with the MB and Rh6G dyes are shown in Figure 8(c, d). The NiO nanoflowers show excellent photodegradation toward MB and R6G under UV light irradiation and the efficiencies are 76.5% and 92.6% respectively.

The relationship between the removal of different cationic dyes and the irradiation time using the NiO nanoflower photocatalyst, demonstrates the gradual decrease in the dye concentration as time increased. The concentration of the dyes in the solution was reduced to 76.5% and 92.6% after 40 & 70 minutes for MB and Rh6G respectively. Due to the increase in the formation of superoxide radicals and hydroxyl radicals over time by the higher specific surface area[68–70] of the NiO nanoflowers, the degradation of the MB and Rh6G molecules get facilitated, thereby allowing their effective photodegradation.

Conclusion

NiO nanoflowers were successfully synthesized by facile hydrothermal process under mild reaction medium, by varying the amount of citric acid used as surfactant. Structural analysis reveals the phase purity, crystallinity and face centered cubic nature of the designed NiO nanoflowers. The average crystalline size was calculated by Debye Scherrer formula and the values (8 nm, 9 nm, 7 nm and 7.5 nm for NiO nanoflowers synthesized with 0.5 g, 1 g, 1.5 g and 2 g of citric acid respectively) are compared with the Williamson Hall plot. The distinct and well-aligned floral microspheres containing nanosheets of NiO was confirmed by the morphological analysis. The proposed growth mechanism of the flower-like morphology elucidates the growth of nanostructure based on self-assembly process. Furthermore, the photocatalytic activity of the synthesized NiO nanoflower was examined during the degradation of MB and Rh6G under UV irradiation. The effective degradation of 75.6% and 92.6% of various cationic dyes by the nanoflowers was explained in detail. In conclusion, the formation of flower-like nanostructure was controlled by the amount of citric acid used which acts as a promoter for the growth process.

Disclosure statement

No potential conflict of interest was reported by the authors.

Funding

No financial support of this work.

References

1. Vidotti, M.; Greco, C. V.; Ponzio, E. A.; Torresi, S. I. C. Sonochemically Synthesized $Ni(OH)_2$ and $Co(OH)_2$ Nanoparticles and Their Application in Electrochromic Electrodes. *Electrochem. Commun.* **2006**, *8*, 554–560. DOI: 10.1016/j.elecom.2006.01.024.
2. Zhou, D.; Yan, A.; Wu, Y.; Wu, T. A Facile Synthetic Route to Flower- like NiO and Its Catalytic Properties. *Indian J. Chem. Sec. A* **2013**, *52*, 51–56.
3. Hotovy, I.; Huran, J.; Spiess, L.; Hascik, S.; Rehacek, V. Preparation of Nickel Oxide Thin Films for Gas Sensors Applications. *Sens. Actuators* **1999**, *57*, 147–152. DOI: 10.1016/S0925-4005(99)00077-5.
4. Hotovy, I.; Rehacek, V.; Siciliano, P.; Capone, S.; Spiess, L. Sensing Characteristics of NiO Thin Films as NO_2 Gas Sensor. *Thin Solid Films* **2002**, *418*, 9–15. DOI: 10.1016/S0040-6090(02)00579-5.
5. Nguyen, D. H.; El-Safty, S. A. Synthesis of Mesoporous NiO Nanosheets for the Detection of Toxic NO_2 Gas. Chemistry **2011**, *17*, 12896–12901. DOI: 10.1002/chem.201101122.
6. Wei, T. Y.; Chen, C. H.; Chien, H. C.; Lu, S. Y.; Hu, C. C. A Cost Effective Supercapacitor Material of Ultrahigh Specific Capacitances: Spinel Nickel Cobaltite Aerogels from an Epoxide-Driven Sol – Gel Process. *Adv. Mater.* **2010**, *22*, 347–351. DOI: 10.1002/adma.200902175.
7. Wang, D. W.; Li, F.; Cheng, H. M. Hierarchical Porous Nickel Oxide and Carbon as Electrode Materials for Asymmetric Supercapacitor. *J. Power Sources* **2008**, *185*, 1563–1568. DOI: 10.1016/j.jpowsour.2008.08.032.
8. Fominykh, K.; Feckl, J. M.; Sicklinger, J.; Döblinger, M.; Böcklein, S.; Ziegler, J.; Peter, L.; Rathousky, J.; Scheidt, E. W.; Bein, T.; Fattakhova-Rohlfing, D. Ultrasmall Dispersible Crystalline Nickel Oxide Nanoparticles as High-Performance Catalysts for Electrochemical Water Splitting. *Adv. Funct. Mater.* **2014**, *24*, 3123–3129. DOI: 10.1002/adfm.201303600.
9. Zhang, F. B.; Zhou, Y. K.; Li, H. L. Nanocrystalline NiO as an Electrode Material for Electrochemical Capacitor. *Mater. Chem. Phys.* **2004**, *83*, 260–264. DOI: 10.1016/j.matchemphys.2003.09.046.
10. Zhao, B.; Ke, X. K.; Bao, J. H.; Wang, C. L.; Dong, L.; Chen, Y. W.; Chen, H. L. Synthesis of Flower-Like NiO and Effects of Morphology on Its Catalytic Properties. *J. Phys. Chem. C.* **2009**, *113*, 14440–14447. DOI: 10.1021/jp904186k.
11. Kim, T. W.; Hwang, S. J.; Jhung, S. H.; Chang, J. S.; Park, H.; Choi, W.; Choy, J. H. Bifunctional Heterogeneous Catalysts for Selective Epoxidation and Visible Light Driven Photolysis: Nickel Oxide Containing Porous Nanocomposite. *Adv. Mater.* **2008**, *20*, 539–542. DOI: 10.1002/adma.200701677.
12. Liu, H.; Wang, G.; Liu, J.; Qiao, S.; Ahn, H. Highly Ordered Mesoporous NiO Anode Material for Lithium Ion Batteries with an Excellent Electrochemical Performance. *J. Mater. Chem.* **2011**, *21*, 3046–3052. DOI: 10.1039/c0jm03132a.
13. Wang, X.; Yang, Z.; Sun, X.; Li, X.; Wang, D.; Wang, P.; He, D. NiO Nanocone Array Electrode with High Capacity and Rate Capability for Li-Ion Batteries. *J. Mater. Chem.* **2011**, *21*, 9988–9990. DOI: 10.1039/c1jm11490e.
14. Gillaspie, D. T.; Tenent, R. C.; Dillon, A. C. Metal-Oxide Films for Electrochromic Applications: Present Technology and Future Directions. *J. Mater. Chem.* **2010**, *20*, 9585–9592. DOI: 10.1039/c0jm00604a.
15. Svensson, J. S. E. M.; Granqvist, C. G. Electrochromic Hydrated Nickel Oxide Coatings for Energy Efficient Windows: Optical Properties and Coloration Mechanism. *Appl. Phys. Lett.* **1986**, *49*, 1566–1568. DOI: 10.1063/1.97281.
16. Yuan, Y. F.; Xia, X. H.; Wu, J. B.; Chen, Y. B.; Yang, J. L.; Guo, S. Y. Enhanced Electrochromic Properties of Ordered Porous Nickel Oxide Thin Film Prepared by Self-Assembled Colloidal Crystal Template-Assisted Electrodeposition. *Electrochim. Acta* **2011**, *56*, 1208–1212. DOI: 10.1016/j.electacta.2010.10.097.

17. Davar, F.; Fereshteh, Z.; Salavati-Niasari, M. Nanoparticle Ni and NiO: Synthesis, Characterization and Magnetic Properties. *J. Alloys Comp.* **2009**, *476*, 797–801. DOI: 10.1016/j.jallcom.2008.09.121.
18. Rueckes, T.; Kim, K.; Joselevich, E.; Tseng, G. Y.; Cheung, C. L.; Lieber, C. M. Carbon Nanotube-Based Nonvolatile Random Access Memory for Molecular Computing. *Science* **2000**, *289*, 94. DOI: 10.1126/science.289.5476.94.
19. Cui, Y.; Lieber, C. M. Functional Nanoscale Electronic Devices Assembled Using Silicon Nanowire Building Blocks. *Science* **2001**, *291*, 851. DOI: 10.1126/science.291.5505.851.
20. Klimov, V. I. Spectral and Dynamical Properties of Multiexcitons in Semiconductor Nanocrystals. *Annu. Rev. Phys. Chem.* **2007**, *58*, 635–673. DOI: 10.1146/annurev.physchem.58.032806.104537.
21. Li, L.; Hu, J.; Yang, W.; Alivisatos, A. P. Band Gap Variation of Size- and Shape-Controlled Colloidal CdSe Quantum Rods. *Nano Lett.* **2001**, *1*, 349–351. DOI: 10.1021/nl015559r.
22. Sa, J.; Kayser, Y.; Milne, C. J.; Fernandes, D. L. A.; Szlachetko, J. Temperature-Programmed Reduction of NiO Nanoparticles Followed by Timeresolved RIXS. *Phys. Chem. Chem. Phys.* **2014**, *16*, 7692–7696.
23. Bita, I.; Yang, J. K. W.; Jung, Y. S.; Ross, C. A.; Thomas, E. L.; Berggren, K. K. Graphoepitaxy of Self-Assembled Block Copolymers on Two-Dimensional Periodic Patterned Templates. *Science* **2008**, *321*, 939. DOI: 10.1126/science.1159352.
24. Cheng, J. J.; Mayes, A. M.; Ross, C. A. Nanostructure Engineering by Template Self-Assembly of Block Copolymers. *Nat. Mater.* **2004**, *3*, 823–828. DOI: 10.1038/nmat1211.
25. CöLfen, H.; Mann, S. Higher-Order Organization by Mesoscale Self-Assembly and Transformation of Hybrid Nanostructures. *Angew. Chem., Int. Ed.* **2003**, *42*, 2350.
26. Zhu, Z.; Wei, N.; Liu, H.; He, Z. Microwave-Assisted Hydrothermal Synthesis of Ni $(OH)_2$ Architectures and Their in Situ Thermal Convention to NiO. *Adv. Powder Technol.* **2011**, *22*, 422–426. DOI: 10.1016/j.apt.2010.06.008.
27. Wang, L.; Zhao, Y.; Lai, Q.; Hao, Y. Preparation of 3D Roselike NiO Complex Structure and Its Electrochemical Property. *J. Alloys Comp.* **2010**, *495*, 82–87. DOI: 10.1016/j.jallcom.2010.01.091.
28. Meher, S. K.; Justin, P.; Rao, R. Microwave-Mediated Synthesis for Improved Morphology and Pseudocapacitance Performance of Nickel Oxide. *ACS Appl. Mater. Interfaces.* **2011**, *3*, 2063–2073. DOI: 10.1021/am200294k.
29. Shende, P.; Kasture, P.; Gaud, R. S. Nanoflowers: The Future Trend of Nanotechnology for Multi-Applications. J. Artificial Cells, *Nanomed. Biotechnol.* **2018**, *46*, 413–422.
30. Li, M.; Schnablegger, H.; Mann, S. Coupled Synthesis and Self-Assembly of Nanoparticles to Give Structures with Controlled Organization. *Nature* **1999**, *402*, 393–395. DOI: 10.1038/46509.
31. Kwan, S.; Kim, F.; Akana, J.; Yang, P. Synthesis and Assembly of $BaWO_4$ Nanorods. *Chem. Commun.* **2001**, *5*, 447–448.
32. Lao, J. Y.; Wen, J. G.; Ren, Z. F. Hierarchical ZnO Nanostructures. *Nano Lett.* **2002**, *2*, 1287–1291. DOI: 10.1021/nl025753t.
33. Shi, H.; Qi, L.; Ma, J.; Cheng, H. H. Polymer-Directed Synthesis of Penniform BaWO4 Nanostructures in Reverse Micelles. *J. Am. Chem. Soc.* **2003**, *125*, 3450. DOI: 10.1021/ja029958f.
34. Mohamed, W. S.; Abu-Dief, A. M. Impact of Rare Earth Europium (RE-Eu^{3+}) Ions Substitution on Microstructural, Optical and Magnetic Properties of $CoFe_{2-x}Eu_xO_4$ Nanosystems. Ceram. Int. **2020**, *46*, 16196–16209. DOI: 10.1016/j.ceramint.2020.03.175.
35. Mohamed, W. S.; Alzaid, M.; Abdelbaky, M. S. M.; Amghouz, Z.; García-Granda, S.; Abu-Dief, A. M. Impact of Co^{2+} Substitution on Microstructure and Magnetic Properties of $Co_xZn_{1-x}Fe_2O_4$ Nanoparticles. *Nanomaterials* **2019**, *9*, 1602.
36. Baker, M. A.; Hamid, M. A. A. Transformation Nanostructured Nickel Hydroxide to Nickel Oxide Film by Aqueous Chemical Growth. *AIP Conf. Proc.* **2013**, *1528*, 359–364.
37. Williamson, G. K.; Hall, W. H. X-Ray Line Broadening from Filed Aluminium and Wolfram. *Acta Metall.* **1953**, *1*, 22–31. DOI: 10.1016/0001-6160(53)90006-6.
38. Mote, V. D.; Purushotham, Y.; Dole, B. N. Williamson-Hall Analysis in Estimation of Lattice Strain in Nanometer-Sized ZnO Particles. J. Theor. Appl. Phys. **2012**, *6*, 6–8. DOI: 10.1186/2251-7235-6-6.
39. Cullity, B. D. *Elements of X-Ray Diffraction*; Addison-Wesley Publishing Company Inc.: California, **1956**.
40. Zak, A. K.; Abd. Majid, W. H.; Abrishami, M. E.; Yousefi, R. X. Ray Analysis of ZnO Nanoparticles by Williamson-Hall and Size-Strain Plot Methods. *Solid State Sci.* **2011**, *13*, 251–256. DOI: 10.1016/j.solidstatesciences.2010.11.024.
41. Yahmadi, B.; Kamoun, N.; Guasch, C.; Bennaceur, R. Synthesis and Characterization of Nanocrystallined In_2S_3 Thin Films via CBD Technique. Mater. Chem. Phys. **2011**, *127*, 239–247. DOI: 10.1016/j.matchemphys.2011.01.066.
42. Deabate, S.; Fourgeot, F.; Henn, F. Henn. F. X-Ray Diffraction and Micro-Raman Spectroscopy Analysis of New Nickel Hydroxide Obtained by Electrodialysis. *J. Power Sources* **2000**, *87*, 125–136. DOI: 10.1016/S0378-7753(99)00437-1.
43. Kiran, N. P.; Deshpande, M. P.; Krishna, C.; Piyush, R.; Vasant, S.; Swati, P.; Chaki, S. H. Synthesis, Structural and Photoluminescence Properties of Nanocrystalline Cu Doped NiO. *Mater. Res. Express* **2017**, *4*, 105027. DOI: 10.1088/2053-1591/aa90ad.
44. Ravikumar, P.; Kisan, B.; Perumal, A. Enhanced Room Temperature Ferromagnetism in Antiferromagnetic NiO Nanoparticles. *AIP Adv.* **2015**, *5*, 87116. DOI: 10.1063/1.4928426.
45. Liu, S.; Jia, J.; Wang, J.; Liu, S.; Wang, X.; Song, H.; Hu, X. Synthesis of Fe-Doped NiO Nanofibers Using Electrospinning Method and Their Ferromagnetic Properties. *J. Magn. Magn. Mater.* **2012**, *324*, 2070–2074. DOI: 10.1016/j.jmmm.2012.02.017.
46. Mironova-Ulmane, N.; Kuzmin, A.; Grabis, J.; Sildos, I.; Voronin, V. I.; Berger, I. F.; Kazantsev, V. A. Structural and Magnetic Properties of Nickel Oxide Nanopowders. *SSP.* **2010**, *168-169*, 341–344. DOI: 10.4028/www.scientific.net/SSP.168-169.341.
47. Thema, F. T.; Manikandan, E.; Gurib-Fakim, A.; Maaza, M. Single Phase Bunsenite NiO Nanoparticles Green Synthesis by Agathosma Betulina Natural Extract. *J. Alloys Compounds* **2016**, *657*, 655–661. DOI: 10.1016/j.jallcom.2015.09.227.
48. Amor, M. B.; Boukhachem, A.; Labidi, A.; Boubaker, K.; Amlouk, M. Physical Nvestigations on Cd Doped NiO Thin Films along with Ethanol Sensing at Relatively Low Temperature. *J. Alloys Compounds* **2017**, *693*, 490–499. DOI: 10.1016/j.jallcom.2016.09.207.
49. Tauc, J. Optical Properties and Electronic Structure of Amorphous Ge and Si. *Mater. Res. Bull.* **1968**, *3*, 37–46. DOI: 10.1016/0025-5408(68)90023-8.
50. Xia, B.; Lenggoro, I. W.; Okuyama, K. The Roles of Ammonia and Ammonium Bicarbonate in the Preparation of Nickel Particles from Nickel Chloride. *J. Mater. Res.* **2000**, *15*, 2157–2166. DOI: 10.1557/JMR.2000.0311.
51. Yang, Y.; Liang, Y.; Zhang, Z.; Zhang, Y.; Wu, H.; Hu, Z. Morphology Well-Controlled Synthesis of NiO by Solvothermal Reaction Time and Their Morphology-Dependent Pseudocapacitive. *J. Alloy. Compd.* **2016**, *658*, 621–628. DOI: 10.1016/j.jallcom.2015.10.253.
52. Dodd, A. C.; McKinley, A. J.; Saunders, M.; Tsuzuki, T. Effect of Particle Size on the Photocatalytic Activity of Nanoparticulate Zinc Oxide. J. Nanopart. Res. **2006**, *8*, 43–51. DOI: 10.1007/s11051-005-5131-z.
53. Mohamed, W. S.; Abu-Dief, A. M. Synthesis, Characterization and Photocatalysis Enhancement of Eu_2O_3-ZnO Mixed Oxide Nanoparticles. J. Phys. Chem. Solids **2018**, *116*, 375–385. DOI: 10.1016/j.jpcs.2018.02.008.
54. Othman, A. A.; Osman, M. A.; Ali, M. A.; Mohamed, W. S.; Ibrahim, E. M. M. Sonochemically Synthesized Ni-Doped ZnS

Nanoparticles: structural, Optical and Photocatalytic Properties. *J. Mater. Sci. Mater. Electron.* **2020**, *31*, 1752–1767.
55. Daneshvar, N.; Behnajady, M. A.; Asghar, Y. Z. Photooxidative Degradation of 4-Nitrophenol (4-NP) in UV/H2O2 Process: Influence of Operational Parameters and Reaction Mechanism. J. Hazard. Mater. **2007**, *139*, 275–279. DOI: 10.1016/j.jhazmat.2006.06.045.
56. Baruah, S.; Dutta, J. Nanotechnology Applications in Pollution Sensing and Degradation in Agriculture: A Review. Environ. Chem. Lett. **2009**, *7*, 191–204. DOI: 10.1007/s10311-009-0228-8.
57. Tian, H.; Fan, H.; Dong, G.; Ma, L.; Ma, J. NiO/ZnO p–n Heterostructures and Gas Sensing Properties for Reduced Operating Temperature. *RSC Adv.* **2016**, *6*, 109091–109098. DOI: 10.1039/C6RA19520B.
58. Irwin, M. D.; Buchholz, D. B.; Hains, A. W.; Chang, R. P.; Marks, T. J. p-Type Semiconducting Nickel Oxide as an Efficiency-Enhancing Anode Interfacial Layer in Polymer Bulk-Heterojunction Solar Cells. Proceedings of the National Academy of Sciences, **2008**, *105*, 2783–2787.
59. Kumar, S.; Reddy, N. L.; Kushwaha, H. S.; Kumar, A.; Shankar, M. V.; Bhattacharyya, K.; Halder, A.; Krishnan, V. Efficient Electron Transfer across a ZnO-MoS2 -Reduced Graphene Oxide Heterojunction for Enhanced Sunlight-Driven Photocatalytic Hydrogen Evolution. *ChemSusChem* **2017**, *10*, 3588–3603. DOI: 10.1002/cssc.201701024.
60. Natu, G.; Hasin, P.; Huang, Z.; Ji, Z.; He, M.; Wu, Y. Valence Band-Edge Engineering of Nickel Oxide Nanoparticles via Cobalt Doping for Application in p-type Dye-Sensitized Solar Cells. *ACS Appl. Mater. Interfaces* **2012**, *4*, 5922–5929. DOI: 10.1021/am301565j.
61. Kumar, S.; Kumar, A.; Kumar, A.; Balaji, R.; Krishnan, V. Highly Efficient Visible Light Active 2D-2D Nanocomposites of N-ZnO-g-C_3N_4 for Photocatalytic Degradation of Diverse Industrial Pollutants. *ChemistrySelect* **2018**, *3*, 1919–1932. DOI: 10.1002/slct.201703156.
62. Kumar, A.; Reddy, K. L.; Kumar, S.; Kumar, A.; Sharma, V.; Krishnan, V. Rational Design and Development of Lanthanide-Doped $NaYF_4$@CdS–Au–RGO as Quaternary Plasmonic Photocatalysts for Harnessing Visible– near-Infrared Broadband Spectrum. *ACS Appl. Mater. Interfaces.* **2018**, *10*, 15565–15581.
63. Kumar, A.; Kumar, S.; Bahuguna, A.; Kumar, A.; Sharma, V.; Krishnan, V. Recyclable, Bifunctional Composites of Perovskite Type N-$CaTiO_3$ and Reduced Grapheme Oxide as an Efficient Adsorptive Photocatalyst for Environmental Remediation. *Mater. Chem. Front.* **2017**, *1*, 2391–2404. DOI: 10.1039/C7QM00362E.
64. Kumar, S.; Sharma, R.; Sharma, V.; Harith, G.; Sivakumar, V.; Krishnan, V. Role of RGO Support and Irradiation Source on the Photocatalytic Activity of CdS–ZnO Semiconductor Nanostructures. *Beilstein J. Nanotechnol.* **2016**, *7*, 1684–1697. DOI: 10.3762/bjnano.7.161.
65. Greiner, M. T.; Helander, M. G.; Wang, Z. B.; Tang, W. M.; Lu, Z. H. Effects of Processing Conditions on the Work Function and Energy-Level Alignment of NiO Thin Films. *J. Phys. Chem. C.* **2010**, *114*, 19777–19781. DOI: 10.1021/jp108281m.
66. Banerjee, S.; Gopal, J.; Muraleedharan, P.; Tyagi, A. K.; Raj, B. Physics and Chemistry of Photocatalytic Titanium Dioxide: Visualization of Bactericidal Activity Using Atomic Force Microscopy. *Curr. Sci.* **2006**, *90*, 1378–1383.
67. Yang, L.; Dong, S.; Sun, J.; Feng, J.; Wu, Q.; Sun, S. Microwave-Assisted Preparation, Characterization and Photocatalytic Properties of a Dumbbell-Shaped ZnO Photocatalyst. *J. Hazard. Mater.* **2010**, *179*, 438–443. DOI: 10.1016/j.jhazmat.2010.03.023.
68. Elmolla, E. S.; Chaudhuri, M. Degradation of Amoxicillin, Ampicillin and Cloxacillin Antibiotics in Aqueous Solution by the UV/ZnO Photocatalytic Process. *J. Hazard. Mater.* **2010**, *173*, 445–449. DOI: 10.1016/j.jhazmat.2009.08.104.
69. Hayat, K.; Gondal, M.; Khaled, M. M.; Ahmed, S.; Shemsi, A. M. Nano ZnO Synthesis by Modified Sol Gel Method and Its Application in Heterogeneous Photocatalytic Removal of Phenol from Water. *Appl. Catal. A* **2011**, *393*, 122–129. DOI: 10.1016/j.apcata.2010.11.032.
70. Tian, C.; Zhang, Q.; Wu, A.; Jiang, M.; Liang, Z.; Jiang, B.; Fu, H. Cost-Effective large-Scale Synthesis of ZnO Photocatalyst with Excellent Performance for Dye Photodegradation. *Chem. Commun. (Camb)* **2012**, *48*, 2858–2860.